






Open Archive TOULOUSE Archive Ouverte (OATAO)

OATAO is an open access repository that collects the work of Toulouse researchers and makes it freely available over the web where possible.

This is an author-deposited version published in : <http://oatao.univ-toulouse.fr/>
Eprints ID : 20116

To link to this article : DOI:10.1063/1.5031780
URL : <http://dx.doi.org/10.1063/1.5031780>

To cite this version : Monrolin, Nicolas  and Praud, Olivier  and Plouraboué, Franck  *Revisiting the positive DC corona discharge theory: Beyond Peek's and Townsend's law.* (2018) Physics of Plasmas, vol. 25 (n° 6). pp. 06350/13-06350/14. ISSN 1070-664X

Any correspondence concerning this service should be sent to the repository administrator: staff-oatao@listes-diff.inp-toulouse.fr

Revisiting the positive DC corona discharge theory: Beyond Peek's and Townsend's law

Nicolas Monrolin, Olivier Praud, and Franck Plouraboué

*Institut de Mécanique des Fluides de Toulouse (IMFT), Université de Toulouse, CNRS, INPT, UPS,
Allée du Pr. Camille Soula, 31400 Toulouse, France*

The classical positive Corona Discharge theory in a cylindrical axisymmetric configuration is revisited in order to find analytically the influence of gas properties and thermodynamic conditions on the corona current. The matched asymptotic expansion of Durbin and Turyn [J. Phys. D: Appl. Phys. **20**, 1490–1495 (1987)] of a simplified but self-consistent problem is performed and explicit analytical solutions are derived. The mathematical derivation enables us to express a new positive DC corona current-voltage characteristic, choosing either a dimensionless or dimensional formulation. In dimensional variables, the current voltage law and the corona inception voltage explicitly depend on the electrode size and physical gas properties such as ionization and photoionization parameters. The analytical predictions are successfully confronted with experiments and Peek's and Townsend's laws. An analytical expression of the corona inception voltage φ_{on} is proposed, which depends on the known values of physical parameters without adjustable parameters. As a proof of consistency, the classical Townsend current-voltage law $I = C\varphi(\varphi - \varphi_{on})$ is retrieved by linearizing the non-dimensional analytical solution. A brief parametric study showcases the interest in this analytical current model, especially for exploring small corona wires or considering various thermodynamic conditions.

I. INTRODUCTION

Corona Discharge (CD) is useful in many valuable applications such as electrostatic precipitators, ozonizers or micro-heat coolers and, for this reason, has been quite extensively studied. CD is a special example of localized gas discharge, for which, in the vicinity of high-tension wires, the ionization of various ionic species is generated by electron collisions. Furthermore, the finite extension of CD in the high-electric field region is edged by vanishing free-electrons resulting from secondary processes such as photo-ionizing radiation produced inside the CD region. The intimate physico-chemical description of CD is thus quite complex, the details of which also depend on the gas composition, the temperature and the physical properties of generated ions. Nevertheless, albeit this complexity is attested, it did not prevent many simplified models to be successfully compared with experimental measurements,^{1–6} to cite only a few. But, all of them derive only implicit current-voltage laws. In order to investigate the capabilities of corona discharge for new applications, there is a growing need for simplified models. For applications involving small emitting electrodes, such as ionic wind devices,^{7,8} an analytical model of the corona discharge current would be a valuable tool.

The current-voltage characteristic $I = f(V)$ is a key property of most corona discharge devices. The case of cylindrical geometry provides a nice configuration for testing a model's prediction. It is characterized by two features: the “starting point,” e.g., onset voltage, and its “shape,” e.g., of $I = f(V)$.

The onset voltage is classically computed from the early phenomenological Peek's law⁹ propounding the critical

electric field E_a at the emitter surface, in cylindrical geometry, in air. Peek's law, however, suffers from providing a purely phenomenological dependency of the critical electric field E_a on emitter's radius a , and is restricted to CD in air in atmospheric conditions for relatively large wires. This is why many theoretical studies have been dedicated to improve the basic knowledge about CD in order to predict the critical electric field and its dependency on the geometrical and physical parameters, in a more general context. More generally, the critical electric field E_a can be obtained from numerically solving the implicit breakdown criterion, e.g., Refs. 10–12 $\int \alpha - \eta = K$, in good agreement with experiments. Nevertheless, some analytical solution to this problem is also interesting since it provides a direct insight into the influence of each parameter. For example, Lowke *et al.*^{13,14} were able to recover an expression similar to Peek's law by injecting a quadratic fit of the ionization coefficient $\alpha(E/N) - \eta(E/N)$ at low E/N into the breakdown criterion.

Now, considering the “shape” of the current-voltage curve, many applications of the corona discharge require accurate current predictions, and simplified corona models are crucial for exploring new applications at low computational cost. Approximations such as two-scale models^{15,16} or perturbative approaches^{17,18} are often confronted by the widely accepted quadratic law derived by Townsend¹⁹ one century ago. However, according to his own words,²⁰ the quadratic equation applies only for “small currents,” otherwise an implicit expression should be used. In order to analytically derive the current, “compartmental” models were developed by involving a corona radius r_i . It has influenced many modeling for which this key parameter permits one to

TABLE I. Effective ionization $\alpha_{ef} = \alpha - \eta$ coefficient fitted from Bolsig+ solver.

	Air ($N_2 + O_2$)	O_2	N_2	$98N_2 + 2CH_4$
C_{ef} ($V\ m^2$)	8.52×10^{-19}	7.93×10^{-19}	8.48×10^{-19}	8.62×10^{-19}
B_{ef} (m^2)	2.93×10^{-20}	4.60×10^{-20}	2.54×10^{-20}	2.90×10^{-20}

separate two distinct phenomenological regions: the “glow discharge” region nearby the emitter and the “drift” region away from it, at the interface of which the continuity of the electrical field is prescribed.^{2,5,21} Even empirically successful and interesting, these “compartmental models” of CD cannot predict the dependency of the critical electric field E_a or the total current I without further assumptions on the exact location of the corona radius r_i . The choice of r_i affects the solution.⁵

On the contrary, in a seminal contribution, Durbin and Turyn¹ re-considered the CD problem in the framework of matched asymptotic analysis. Their approach has enabled them to obtain the relationship between the CD region relative size (relative to some typical length in the drift region) and some typical ionization electric field E_i to be defined later. Durbin and Turyn¹ also numerically solved the matching condition so as to produce a new theoretical prediction for the (dimensionless) current-voltage $I = f(V)$. Unfortunately, their theoretical predictions have been poorly confronted by experimental measurements. Furthermore, they only solve the matching conditions numerically and did not produce any explicit results on how their theoretical predictions associated with the critical electric field or the current-voltage characteristics depends on physical parameters.

In this contribution, we revisit the Durbin and Turyn¹ matched asymptotic approach to a positive CD cylindrical problem and extend it to a more general framework. An explicit analytical solution for the matching conditions is found. This permits us to easily evaluate the impact of each physical parameter such as effective mobility, ionization, photo-ionization or electrode size on the corona current and onset. The analytical current-voltage $I = f(V)$ is found, which, in the limit of small currents, exactly derives Townsend’s law $I = C\varphi(\varphi - \varphi_{on})$. The theoretical predictions are analyzed in various ways: (i) their ability to predict current-voltage characteristics in different gases as compared with experimental measurements, (ii) their validity range as compared with Townsend’s law, (iii) the quality of the asymptotic approximation and (iv) the dependency of the produced current on physical parameters such as thermodynamic conditions.

This paper is organized as follows: first, the simplified constitutive equations of CD are presented in Sec. II. Then, their dimensionless formulation is presented in Sec. II A and their mathematical asymptotic analysis in Secs. II B and II C. Section III describes how the theoretical predictions of Sec. II can be analyzed in a dimensionless (Sec. III A) or dimensional formulation (Sec. III B), so as to assess the quality of the asymptotic approximation and how they compare with Peek’s law or other onset criteria for corona onset and Townsend’s law for current. In Sec. III C, the analytical

solution is compared with current-voltage measurements under various gas conditions. Section III C 1 discusses the validity and limits of the analytical shape of the effective ionization coefficient. Finally, Sec. IV showcases the applications of the presented analytical model with a brief parametric study.

II. PHYSICAL MODEL AND METHOD

The matched asymptotic method is used to solve equations with physical processes that are dominant in some region (a boundary layer) and negligible elsewhere. In their analysis, Durbin and Turyn¹ have mathematically shown that the corona problem has two distinct regions: an inner and an outer region. In the inner region, they show that the leading order of the electrical potential solution is harmonic (no space charge effects) which greatly simplifies the computation of the source terms for charge production caused by electronic impact and attachment. This is the “glow corona” region. The charge-free potential is often employed at the inception voltage,^{6,10–12} but Durbin and Turyn proved that it still holds at higher voltages. However, the “boundary condition” at the edge of the inner region depends on the solution in the outer region, which make the inner solution not completely independent of space charge effects. In the outer region, the concentration of electrons is found to be evanescent, the positive charges are electro-convected, and coupled with the electrical potential through the classical electrostatic Poisson problem (not harmonic in this region). This outer region is the “drift” region. In Fig. 1, an intermediate zone is introduced, to be discussed in the mathematical matching section.

A. Governing equations

As mentioned in the Introduction, the effective fluid model of the positive DC corona is considered. The

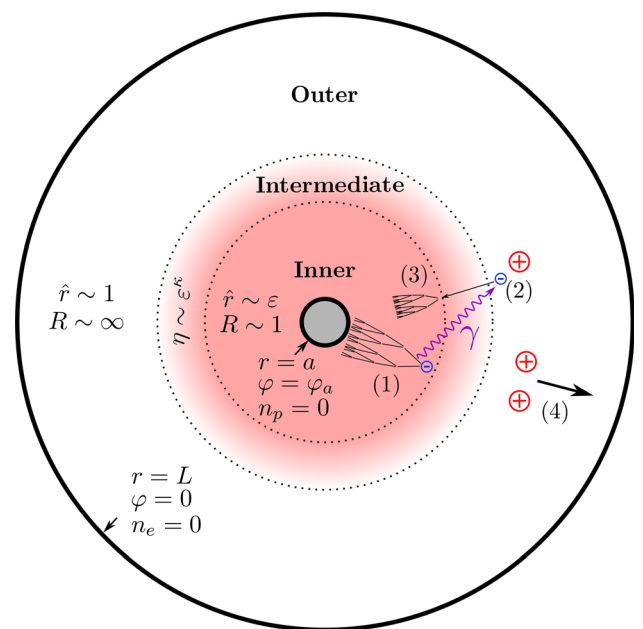


FIG. 1. Coaxial electrode geometry, asymptotic regions and the corresponding physical processes. (1) Primary electron avalanche, (2) secondary ionization, (3) secondary electron avalanche, and (4) ion drift.

production of positive ions, electrons and negative ions (with respective densities n_p , n_e and n_n) is governed by the impact ionization coefficient α and the attachment coefficient η . The ionization coefficient dependency on the electric field will take the standard Townsend form

$$\alpha = \beta e^{-E_i/E}, \quad (1)$$

where β and E_i are two physical parameters which depend on the gas composition and thermodynamic conditions and are supposed to be known. The attachment coefficient is assumed to vanish in low electric fields. Section III C 1 provides more information about how they were evaluated and under which conditions relation (1) is accurate and reliable. Hence, combining the previous effects provides the following constitutive model:

$$\nabla^2 \varphi = \frac{e}{\epsilon_0} (n_e + n_n - n_p), \quad (2)$$

$$\nabla \cdot \mathbf{j}_p = \alpha \|\mathbf{j}_e\| + S, \quad (3)$$

$$\nabla \cdot \mathbf{j}_e = (\alpha - \eta) \|\mathbf{j}_e\| + S, \quad (4)$$

$$\nabla \cdot \mathbf{j}_n = \eta \|\mathbf{j}_e\|, \quad (5)$$

where e is the elementary charge, $\mathbf{j}_e = \mu_e n_e \nabla \varphi$, $\mathbf{j}_p = -\mu_p n_p \nabla \varphi$, and $\mathbf{j}_n = \mu_n n_n \nabla \varphi$ are the local fluxes of the electrons, positive and negative charges, respectively. One complex aspect of CD modeling concerns the generation of secondary electrons. Even if secondary ionization is very small compared to the impact ionization, it is necessary to explain the onset of the discharge. Here, the photo-ionization is the main source of secondary electrons

$$S(\mathbf{r}) = \lambda \gamma \int_V G(\mathbf{r}, \mathbf{r}') (\alpha(r') - \eta(r')) \|\mathbf{j}_e(\mathbf{r}')\| d^3 \mathbf{r}'. \quad (6)$$

$S(\mathbf{r})$ is the number of photo-ionizing events at position \mathbf{r} per unit time and volume. The coefficient γ is the secondary electron efficiency, identical to the one introduced by Zheng.²² The effective absorption coefficient is named λ (and not μ as in Refs. 1 and 22 to avoid confusion with mobility) and $\lambda G(\mathbf{r}, \mathbf{r}')$ is its associated effective absorption function. The photon absorption function may have different forms^{1,11,23} (for now, no particular shape is assumed).

Following Ref. 1, all quantities are rescaled with the radius of the collector L , the positive ion mobility μ_p , the applied voltage φ_a and the net current I per unit length at the collector to build the following non-dimensional quantities (hat stands for non-dimensional):

$$\hat{r} = \frac{r}{L}, \quad \hat{\varphi} = \frac{\varphi}{\varphi_a}, \quad \hat{n}_k = \frac{n_k}{n_{k,0}}, \quad \hat{a} = \frac{a}{L}, \quad (7)$$

with $n_{k,0} = I/(2\pi\mu_k e \varphi_a)$, $k \equiv e, p, n$, and a the emitter radius. As mentioned by Durbin,¹ the reaction coefficients have to scale as follows:

$$\frac{\hat{\alpha}}{\varepsilon} = L\alpha = \frac{\hat{\beta}}{\varepsilon} e^{-\frac{1}{\varepsilon}},$$

$$\frac{\hat{\eta}}{\varepsilon} = L\eta,$$

with $\hat{\beta} = \beta L \varepsilon$. For conciseness, $\hat{\alpha}_{ef} = \hat{\alpha} - \hat{\eta}$ is the effective ionization coefficient. The small asymptotic parameter ε is defined by

$$\varepsilon = \frac{\varphi_a}{LE_i}. \quad (8)$$

A distinct reference density is chosen for the ions and the electrons because, physically, their flux only is expected to match. Hence, the ratio of electron to positive ion density is merely proportional to the inverse ratio of their respective mobilities. Positive and negative ions have similar mobilities $\mu_p \approx \mu_n$. Using this non-dimensional formulation, the governing equations are now expressed in 2D cylindrical axis-symmetrical configurations. Realizing that the fluxes are radial, so that $\hat{\mathbf{j}}_e = \hat{j}_e \mathbf{e}_r$ and $-\nabla \hat{\varphi} = \hat{E} \mathbf{e}_r$, dimensionless governing equations read as

$$\frac{1}{\hat{r}} \partial_{\hat{r}} (\hat{r} \partial_{\hat{r}} \hat{\varphi}) = -J(\hat{n}_p - \delta_\mu \hat{n}_e - n_n), \quad (9)$$

$$\frac{1}{\hat{r}} \partial_{\hat{r}} (\hat{r} \hat{j}_p) = -\frac{\hat{\alpha}}{\varepsilon} \hat{j}_e - \hat{S}(\hat{r}), \quad (10)$$

$$\frac{1}{\hat{r}} \partial_{\hat{r}} (\hat{r} \hat{j}_e) = -\frac{\hat{\alpha} - \hat{\eta}}{\varepsilon} \hat{j}_e - \hat{S}(\hat{r}), \quad (11)$$

$$\frac{1}{\hat{r}} \partial_{\hat{r}} (\hat{r} \hat{j}_n) = -\frac{\hat{\eta}}{\varepsilon} \hat{j}_e, \quad (12)$$

with $\hat{S}(\hat{r}) = \hat{\lambda} \gamma \int G(\hat{\mathbf{r}}, \hat{\mathbf{r}}') \left[\frac{\hat{\alpha} - \hat{\eta}}{\varepsilon} \hat{j}_e \right](\hat{\mathbf{r}}') d^2 \hat{\mathbf{r}}'$. Note that the volume integral was transformed into a surface integral by integrating along the electrode axis: $G_{2D}(r, \theta) = \int_{-\infty}^{+\infty} G_{3D}(r, \theta, z) dz$. The minus sign on the left-hand-side comes from $|\hat{j}_e| = -\hat{j}_e$, since the voltage gradient is negative. The dimensionless parameter J , acting as a dimensionless current, or space charge parameter, is defined as

$$J = \frac{n_{0,p} L^2}{\epsilon_0 \varphi_a^2} = \frac{IL^2}{2\pi \mu_p \epsilon_0 \varphi_a^2}. \quad (13)$$

Note that contrary to Durbin and Turyn, we differentiate the adimensionalization for ions and electrons, so that $\hat{n}_e \sim \hat{n}_p \sim 1$. This is why the small parameter $\delta_\mu = n_{e,0}/n_{p,0} = \mu_p/\mu_e$ appears in (9). δ_μ typically takes values smaller than 10^{-2} in air.

The mobility of each species can be assumed to be constant without loss of generality. The charge conservation equations (10) and (11) are indeed written in terms of flux and the mobility dependence on the electric field is then transparent for charge conservation equations. Besides, the upcoming Sec. II B states that in the high electric field region, where the mobility most likely varies, the species concentration can be dropped in the potential equation (9).

It is important to mention that the original model considered by Durbin¹ does not present a balanced distribution of the photo-ionization which is only a source term for electrons, but not for positive ions. As a result, the total current produced at the CD edge is not exactly conserved at the inner/outer interface. This issue is more benign than first suggested. As a matter of fact, the current inconsistency scales with the small parameter γ (see Sec. II D 2). The small

photo-ionization efficiency (typically $\gamma < 10^{-3}$) results in a very weak correction to the overall positive ion current. This is completely coherent with previous results²² where the computed positive ion flux is conserved in the outer region, indicating negligible source terms. So, photo-ions can be neglected. The number of negative ions is also a small quantity compared to positive ions. First, the negative ion production rate is very small $n_{n,max}/n_{p,max} \sim \eta/\alpha \ll 1$ and secondly, they are produced only in the inner region, where the space charge will be negligible. For conciseness, the rest of the analysis focuses on the relevant species: positive ions and electrons.

B. Inner expansion

In the inner region, the scaling is small $\hat{r} \sim \varepsilon$. To keep a $O(1)$ space variable, it is rescaled as $R = \hat{r}/\varepsilon$. Every variable \hat{x} is then rewritten, so that $X(R) = \hat{x}(\hat{r})$, where capital letters denote the inner, whereas the hatted ones, the outer. This scaling implies a contraction of both derivatives and the reaction coefficient, i.e.,

$$\partial_R \Phi = \varepsilon \partial_{\hat{r}} \hat{\phi} J_k = \varepsilon \hat{j}_k \hat{\alpha}(\varepsilon R) = \hat{\alpha}(\hat{r}).$$

The set of constitutive equations can then be rewritten as

$$\frac{1}{R} \partial_R (R \partial_R \Phi) = -\varepsilon^2 J (N_p - \delta_\mu N_e), \quad (14)$$

$$\frac{1}{R} \partial_R (R J_p) = -\hat{\alpha} J_e - \varepsilon^2 \hat{\lambda} \gamma \int G \hat{\alpha} J_e d^2 \mathbf{R}', \quad (15)$$

$$\frac{1}{R} \partial_R (R J_e) = -\hat{\alpha} J_e - \varepsilon^2 \hat{\lambda} \gamma \int G \hat{\alpha} J_e d^2 \mathbf{R}'. \quad (16)$$

The solution inside the inner region is sought after from the following double asymptotic expansion resulting from the balance of various terms

$$\Phi = \Phi_0 + \varepsilon \Phi_1 + \frac{1}{\varepsilon} e^{-\frac{\hat{r}}{\varepsilon}} \Phi_2 + \dots, \quad (17)$$

$$N_p = N_{p,0} + \varepsilon N_{p,1} + \frac{1}{\varepsilon} e^{-\frac{\hat{r}}{\varepsilon}} N_{p,2} + \dots, \quad (18)$$

$$N_e = N_{e,0} + \varepsilon N_{e,1} + \frac{1}{\varepsilon} e^{-\frac{\hat{r}}{\varepsilon}} N_{e,2} + \dots. \quad (19)$$

Keeping with the leading order and dropping the index 0 for notation simplicity (whilst obviously consistently ignoring the influence of further terms of the expansion in the following) leads to the leading order inner problem.

$$\frac{1}{R} \partial_R (R \partial_R \Phi) = 0, \quad (20)$$

$$\partial_R \Pi_p = \hat{\alpha}(\varepsilon R) \Pi_e, \quad (21)$$

$$\partial_R \Pi_e = -\hat{\alpha}_{ef}(\varepsilon R) \Pi_e, \quad (22)$$

where we have considered the (normalized) total fluxes $\Pi_k = \frac{1}{2\pi} \int_{C(R)} (\mathbf{J}_k \cdot \mathbf{n}) R d\theta = \pm J_k R$, $k \equiv e, p$.

C. Outer expansion

Let us now consider the outer scaling variable $\hat{r} \sim 1$. In the outer region, the photoionization term can be developed into a classical multi-polar expansion, since the main contribution of the convolution product comes from the contribution of the inner region ($\hat{\mathbf{r}}' = \varepsilon \mathbf{R}'$). This non-local term is expanded with the hierarchy of moments of the electron flux inside the inner region: a mono-polar leading order term associated with the zeroth moment of the electron flux, a bipolar correction associated with the first moment, etc.

$$\begin{aligned} \int G \hat{\alpha} J_e d^2 \mathbf{R}' &= \int G(\hat{\mathbf{r}}, \varepsilon \mathbf{R}') [\hat{\alpha}_{ef} J_e]_{\mathbf{R}'} d^2 \mathbf{R}' \\ &= G(\hat{\mathbf{r}}, 0) \int [\hat{\alpha}_{ef} J_e]_{\mathbf{R}'} d^2 \mathbf{R}' \\ &\quad + \varepsilon \nabla G(\hat{\mathbf{r}}, 0) \cdot \int [\hat{\alpha}_{ef} J_e]_{\mathbf{R}'} \mathbf{R}' d^2 \mathbf{R}' + \dots \end{aligned}$$

In the special case of axi-symmetric solutions, the first order $O(\varepsilon)$ dipole correction cancels. Using a similar asymptotic expansion (17)–(19), in outer constitutive equations (9)–(11), again dropping the index and keeping only the leading-order set of equations, one finds

$$\frac{1}{\hat{r}} \partial_{\hat{r}} (\hat{r} \partial_{\hat{r}} \hat{\phi}) = -J (\hat{n}_p - \delta_\mu \hat{n}_e), \quad (23)$$

$$\partial_{\hat{r}} \hat{\pi}_p = 0, \quad (24)$$

$$\partial_{\hat{r}} \hat{\pi}_e = -2\pi \gamma \hat{r} \hat{\lambda} G(\hat{r}, 0) \int_{a/\varepsilon}^{\infty} \hat{\alpha}_{ef}(\varepsilon R') \Pi_e dR'. \quad (25)$$

The solution for the electron flux $\hat{\pi}_e$ can easily be obtained from integrating (25), given the radiation kernel $G(\hat{r}, 0)$. Following Refs. 1 and 23, an asymptotic cylindrical radiative kernel $G(\hat{r}, 0) = e^{-\hat{r}} / 2\pi \hat{r}$ produces the leading-order electron flux

$$\hat{\pi}_e = -\gamma e^{-\hat{r}} \int_{a/\varepsilon}^{\infty} \hat{\alpha}(\varepsilon R') \Pi_e dR',$$

which provides an evanescent exponentially decaying secondary electron flux in the outer region with a typical decaying length $1/\hat{\lambda}$. Furthermore, both the photo-ionization coefficient γ and the mobility ratio between the electrons and the positive charges are small (again, typically $\delta_\mu \sim 10^{-2} \ll 1$), so that the back-coupling of photo-emitted induced electrons into the electrical potential can be neglected. This issue can be more formally re-casted into searching for a solution given by a second regular asymptotic expansion in the mobility ratio

$$\hat{\phi}_0 = \hat{\phi}_{00} + \delta_\mu \hat{\phi}_{01} + \dots$$

$$n_{p,0} = \tilde{n}_{p,00} + \delta_\mu \tilde{n}_{p,01} + \dots$$

$$n_{e,0} = \tilde{n}_{e,00} + \delta_\mu \tilde{n}_{e,01} + \dots$$

Keeping with the leading order, and again, for notation simplicity, dropping the index leads to re-formulate (23)–(25) into the leading order set of equation

$$\partial_{\hat{r}}(\hat{r}\partial_{\hat{r}}\hat{\phi}) = -J\hat{n}_p, \quad (26)$$

$$\partial_{\hat{r}}\hat{\pi}_p = 0, \quad (27)$$

which are, in fact, the classical ‘‘drift’’ region equations for which the influence of the electron charges is neglected. This set of equation can be solved analytically, but some constant will remain undetermined, like the non-dimensional parameter J . A complete solution can be obtained by matching the outer and inner sets of solutions.

D. Matching conditions

The resolution of the inner and outer set of equations is not especially difficult, but for the sake of conciseness, the reader might refer to previous works.^{1,2,5,6,21} Whatever, at this stage, the inner and outer solutions are not fully consistent since they contain four undetermined constants: A , K_1 and J for the potential and $\Pi_{e\infty}$ for the electron, to be defined in the coming section or in Ref. 1. This uncertainty can be overcome by adjusting the inner and outer solutions so that they match in the intermediate zone.

1. Matching for electrons

The inner solution for electrons’ total flux can be written as

$$\Pi_e(R) = \Pi_{e\infty} e^{\left(\int_R^{\infty} \hat{\alpha}_{ef}(\varepsilon R') dR'\right)}.$$

In the outer region, the total flux of electrons can be written as

$$\hat{\pi}_e(\hat{r}) = -\gamma e^{-\hat{\lambda}\hat{r}} \int_{\hat{a}/\varepsilon}^{\infty} \hat{\alpha}_{ef}(\varepsilon R') \Pi_e dR'.$$

The matching condition $\lim_{R \rightarrow \infty} \Pi_e = \lim_{\hat{r} \rightarrow 0} \hat{\pi}_e$ leads to

$$\Pi_{e\infty} = \gamma \int_{\hat{a}/\varepsilon}^{\infty} \hat{\alpha}_{ef} \Pi_e dR'. \quad (28)$$

The integral term can be expressed as the difference between the inner and outer fluxes because, using (22), $\int \alpha_{ef} \Pi_e dR = \int -\partial_R(\Pi_e) dR = \Pi_{e,a} - \Pi_{e\infty}$. Using the inner solution, we substitute $\Pi_{e,a} = \Pi_{e\infty} e^{\left(\int_{\hat{a}/\varepsilon}^{\infty} \alpha_{ef} dR\right)}$, so that the matching condition finally reads

$$\Pi_{e\infty} = \gamma \left[\Pi_{e\infty} e^{\left(\int_{\hat{a}/\varepsilon}^{\infty} \hat{\alpha}_{ef}(\varepsilon R') dR'\right)} - \Pi_{e\infty} \right],$$

which can be rearranged into a Townsend’s like onset criterion

$$\ln(1 + \gamma^{-1}) = \int_{\hat{a}/\varepsilon}^{\infty} \hat{\alpha}_{ef}(\varepsilon R') dR'. \quad (29)$$

This is an implicit condition on the electric field that can be solved numerically.¹⁰ The accurate prediction of the corona onset and especially of the constant $K = \ln(1 + \gamma^{-1})$ is still an ongoing issue.^{11,12} The criterion (29) is nonetheless widely used and remains satisfying for most applications.

2. Matching for ions

The inner solution for ions can be written as

$$\Pi_p(R) = -\Pi_{e\infty} \int_{\hat{a}/\varepsilon}^R \hat{\alpha}(R') e^{\int_{R'}^{\infty} \hat{\alpha} - \hat{\eta} dR''} dR',$$

while in the outer one, the definition of the ion flux $\int_{\hat{r}=1}^{\infty} \hat{\pi}_p d\theta = 2\pi$ is given by

$$\hat{\pi}_p = 1.$$

More precisely, without neglecting photoionization for ions and negative ions, the outer solution should be

$$\hat{\pi}_p = 1 - \hat{\pi}_e - \hat{\pi}_n. \quad (30)$$

But, as shown in the previous Sec. II C, the outer electron flux $\hat{\pi}_e$ is very small since it scales with γ . The negative ion flux is exactly zero because it is zero at the collector (imposed boundary condition) and there is asymptotically no electron attachment in the outer region. So, the matching condition $\lim_{R \rightarrow \infty} N_p = \lim_{\hat{r} \rightarrow 0} \hat{n}_p$ gives the value of the incoming electron flux

$$\Pi_{e\infty} = \left[e^{\int_{\hat{a}/\varepsilon}^{\infty} \hat{\alpha} dR'} - 1 - \int_{\hat{a}/\varepsilon}^{\infty} \eta e^{\int_R^{\infty} \hat{\alpha} - \hat{\eta} dR''} \right]^{-1}. \quad (31)$$

3. Matching for potential

The matching condition for electric potential is more technical than the previous ones. Integrating the Poisson equation gives four constants: two in the inner region and two in the outer. Two constants are determined by applying the boundary conditions in $R = \hat{a}/\varepsilon$ and $\hat{r} = 1$, while the remaining two, J and K_1 , are provided by matching conditions. Durbin¹ applies intuitively conditions on the electric flux $r\partial_r\phi$ and on the potential, which leads to an implicit relationship between the space charge parameter J and the surface electric field parameter A .

$$\int_a^1 \sqrt{J + A^2/r^2} dr = 1. \quad (32)$$

Finding the relationship $J = f(A)$ is tantamount to finding the current-voltage law $I = f(V)$. Here, a more sophisticated, although classical, intermediate variable matching (see Hinch²⁴) is applied. The derivation is summarized in the Appendix. The matching condition is given by

$$1 - A \ln\left(\frac{1}{\hat{a}}\right) = \sqrt{J + A^2} - A + A \ln\left(\frac{2A}{\sqrt{J + A^2} + A}\right), \quad (33)$$

which provides an unambiguous and integrated expression, with rigorous derivation. This implicit law $f(A, J, \hat{a}) = 0$ gives the non-dimensional current J as a function of the non-dimensional surface field A . Solving this equation and extracting the dimensional variables will give the current-voltage law, as shown in Sec. III.

III. RESULTS

The previous matching conditions are further analyzed. The results of practical interest are derived such as the current-voltage and the corona inception field as functions of ionization coefficient and geometry.

A. Non-dimensional results

1. Onset criterion

In order to find an explicit analytical solution for the matching condition, the effective ionization coefficient is assumed to behave like α . Taking $\alpha_{ef} = \beta_{ef} e^{-E_{ief}/E}$ is quite relevant at high electric fields, since α will dominate η , see Sec. III C 1. From (20), the inner electric field is written as $E = -\partial_R \Phi = A/R$ with A to be determined. Injecting the electric field in $\hat{\alpha}_{ef}(\varepsilon R) = \beta_{ef} L \varepsilon e^{-\varepsilon R/(\varepsilon_{ef} A)}$ and integrating lead to a condition similar to the one obtained by Durbin¹

$$\ln(1 + \gamma^{-1}) = A\beta/\varepsilon_{ef} e^{-\hat{a}/(\varepsilon_{ef} A)} \quad (34)$$

but with $\varepsilon_{ef} = \varphi_a/LE_{ief}$. To obtain an explicit expression for A , (34) is rearranged as

$$\frac{\hat{a}\hat{\beta}}{\ln(1 + \gamma^{-1})} = \hat{a}/(\varepsilon_{ef} A) e^{\hat{a}/(\varepsilon_{ef} A)}.$$

A is then expressed with the Lambert \mathcal{W} function,³⁵ see Fig. 2,

$$\mathcal{W} \left(\frac{\hat{a}\beta_{ef}L}{\ln(1 + \gamma^{-1})} \right) = \frac{\hat{a}}{\varepsilon_{ef} A}.$$

Since $\hat{a}\beta_{ef}L/\ln(1 + \gamma^{-1}) > 0$, the branch 0 of the Lambert \mathcal{W} function must be used.

$$A = \hat{a}/\varepsilon_{ef} \left[\mathcal{W}_0 \left(\frac{\hat{a}\beta_{ef}L}{\ln(1 + \gamma^{-1})} \right) \right]^{-1}. \quad (35)$$

In practice, $A = -\hat{a}\partial_f \hat{\varphi}|_{\hat{a}}$ is linked to the surface voltage gradient at the emitter. So, the non-dimensional condition (35) sets the surface electric field as a function of physical parameters \hat{a} , $\beta_{ef}L$ and γ as well as the effective asymptotic

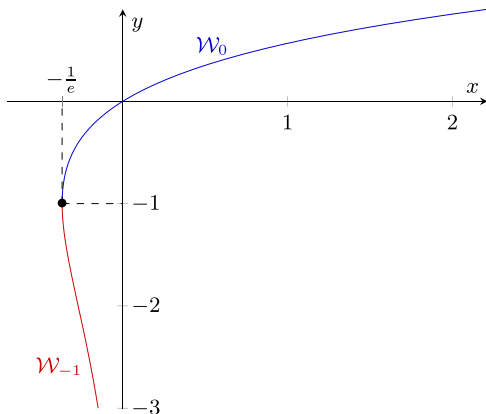


FIG. 2. The real branches of Lambert \mathcal{W} function.

parameter ε_{ef} . The practical consequences of this result are further developed in Sec. III B 1.

2. Non-dimensional current

The matching condition (33) is still an implicit relationship, which does not bring much advantages compared to the previous analytical works^{1,5,25} or numerical methods. It can be rearranged in two ways.

In the first way, notice that

$$V = 1/A \ln(1/\hat{a}) = \varphi_a/aE_a \ln(L/a)$$

which is the ratio between the onset voltage and the applied voltage and that

$$C = J/A^2 = IL^2/(2\pi\mu_p \varepsilon_0 a^2 E_a^2)$$

is proportional to the current I , since E_a is independent of the applied voltage, see Sec. III B 1. Rearranging the matching condition, we obtain

$$V = 1 + \frac{1}{\ln(1/\hat{a})} [1 + \sqrt{C+1} - \ln(1 + \sqrt{C+1}) - (2 - \ln(2))]. \quad (36)$$

This expression gives the reduced voltage V against the reduced current C . Similar results were originally obtained by Thompson and Thompson as explained by Jones,⁵ for example. Their non-dimensional parameters are slightly different since they involve a corona radius as explained earlier, but the analytical expressions are very similar. It matches with the charge injection model such as Zheng *et al.*,¹² as shown in Appendix B.

The second way is less straightforward but more interesting, since it allows to recover an explicit expression of J . First, (36) is reorganized using notations $Y = 1 + \sqrt{C+1}$ and $K = \ln(1/\hat{a})(V-1) + 2 - \ln(2)$

$$K = Y - \ln(Y). \quad (37)$$

Then, exponentiating and arranging lead to

$$e^K = \frac{1}{Y} e^Y, \\ -e^{-K} = -Y e^{-Y}.$$

The solution is given by the Lambert \mathcal{W} function. Applying the definition of \mathcal{W} gives $-Y = \mathcal{W}(-e^{-K})$. Re-injecting C in the expression finally leads to

$$C = [1 + \mathcal{W}_{-1}(-e^{-K})]^2 - 1, \quad (38)$$

or equivalently, using $-e^{-K} = -2e^{-2} (1/\hat{a})^{V-1}$ and injecting J and A

$$\frac{J}{A^2} = \mathcal{F}(-2e^{-2} \hat{a}^{V-1}), \quad (39)$$

with \mathcal{F} being given by

$$\mathcal{F}(x) = [1 + \mathcal{W}_{-1}(x)]^2 - 1. \quad (40)$$

More properties concerning this function \mathcal{W} can be found in Ref. 26, for example. Three remarks concern this solution.

- For a particular value $A \ln(1/\hat{a}) = 1$, the space charge equals zero $J = 0$. In dimensional variables, the condition is written as $aE_a \ln(L/a)/\varphi_a = 1$ or $\varphi_a = aE_a \ln(L/a)$. This corresponds to the charge free solution for electric potential which holds only at the corona inception point.
- $-e^{-K} < 0$ and $\mathcal{W}(x)$ has two real branches when $x \in [-1/e, 0]$, see Fig. 2. Only the branch \mathcal{W}_{-1} gives positive values of J . The branch 0 is also a solution, but provides negative values of J , which is not relevant to the case considered here. Nevertheless, this further branch might be of interest when considering dynamical solutions associated with the stability of CD, for example.
- This equation admits a real solution, only if $-e^{-K} \geq -1/e$. The solution is complex otherwise. This condition writes $\frac{1}{A} \geq \ln(2/\hat{a}) - 1$, which is a condition on the voltage and the electric field at the emitting electrode in dimensional variables $\frac{\varphi_a}{aE_a} \geq \ln(2L/a) - 1$. Once again, obtaining negative values of J , below the inception condition, is not obvious to interpretation.

The corona inception point $J = 0$ is of particular interest. Since the Taylor expansion of \mathcal{W} is rather fastidious,²⁶ software Maple is used to compute the first five orders. The expansion of J around the point $A = 1/\ln(1/\hat{a})$ with $X = A - 1/\ln(1/\hat{a})$ is then written as

$$J = -4X + 2 \ln(\hat{a})(2 + \ln(\hat{a}))X^2 + \frac{2}{3} \ln(\hat{a})^4 X^3 + \frac{1}{6} \ln(\hat{a})^5 (5 \ln(\hat{a}) + 4)X^4 + \frac{1}{30} \ln(\hat{a})^6 (41 \ln(\hat{a})^2 + 50 \ln(\hat{a}) + 20)X^5 + O(X^6). \quad (41)$$

The consecutive expansion orders are plotted in Fig. 3. Increasing the order of expansion does not provide much progress, since the high order terms strongly diverge far from $J = 0$. It is interesting that $J(A)$ can be linearly approximated with the universal slope -4 . The validity range of the

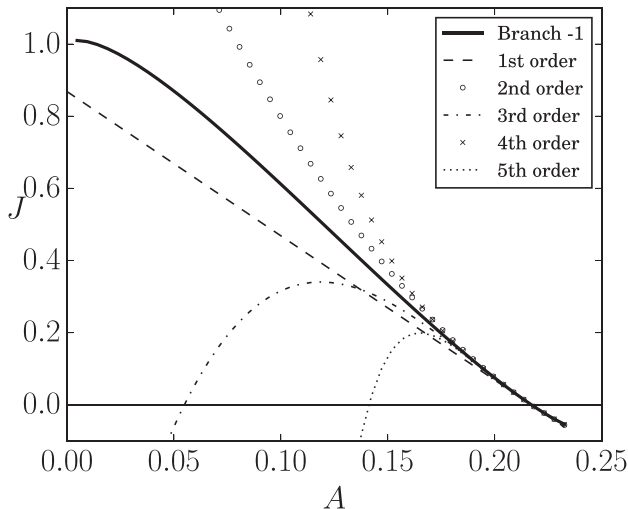


FIG. 3. Matching condition for J and A for $\hat{a} = 10^{-2}$ and the first terms of the Taylor expansion (41).

linearized law, Fig. 4, decreases as \hat{a} decreases. This is because the second order term of the Taylor expansion scales as $\ln(\hat{a})^2$. This has practical consequences concerning the well-known Townsend law, as further discussed in Sec. III B 2.

B. Dimensional laws

1. Onset electric field expression

Injecting the dimensional variables $\hat{a} = a/L$ and $A = aE_a/\varphi_a$ into (35) gives the inception voltage as a function of the gas ionization properties and the emitter radius

$$E_a = E_{ief} \left[\mathcal{W}_0 \frac{a\beta_{ef}}{\ln(1 + \gamma^{-1})} \right]^{-1}. \quad (42)$$

It is quite interesting to note that, for the leading order solution considered here, the surface electric field E_a does not depend on the applied voltage φ_a , but only on the gas properties and geometry. Equation (42) is similar to the well-known Peek's law, since it provides the value of the surface electric field versus the emitter diameter. As a reminder, Peek's law is written as⁹

$$E_a = 3.1 \times 10^6 \delta \left(1 + \frac{0.0308}{\sqrt{\delta a}} \right) \text{ (V/m)}, \quad (43)$$

with a density correction factor $\delta = N/N_0$ and $N_0 = 2.5 \times 10^{25} \text{ m}^{-3}$ with the standard air density at 298 K and 1013.25 hPa. Since (42) relies on the electron matching condition, similar to the classical onset criterion, it directly involves the ionization coefficient. By fitting α_{ef} in air, see Sec. III C 1, and we obtain the critical surface electric field. The comparison, Fig. 5, shows that the matching condition is very similar to Peek's law for relatively large corona wires ($0.1 \text{ mm} < a < 1 \text{ cm}$) with an agreement of less than 5%. This corresponds to the range covered by the experimental data used by Peek⁹ to fit the well-known empirical law (Fig. 5).

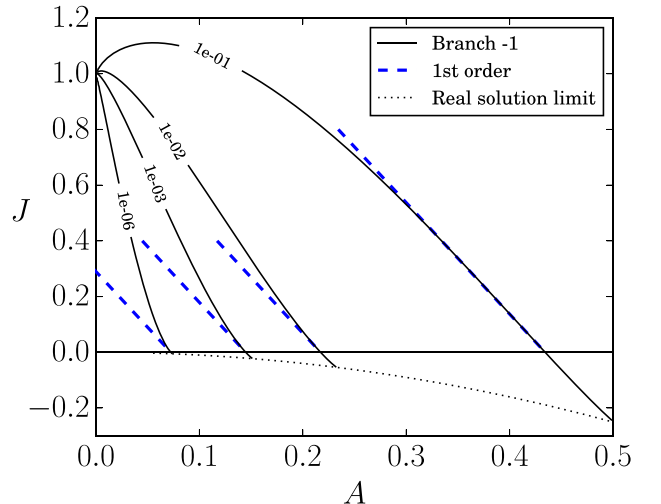


FIG. 4. Analytical solution $J = f(A)$ for various emitter diameters: $\hat{a} \in [10^{-6}; 10^{-3}; 10^{-2}; 10^{-1}]$.

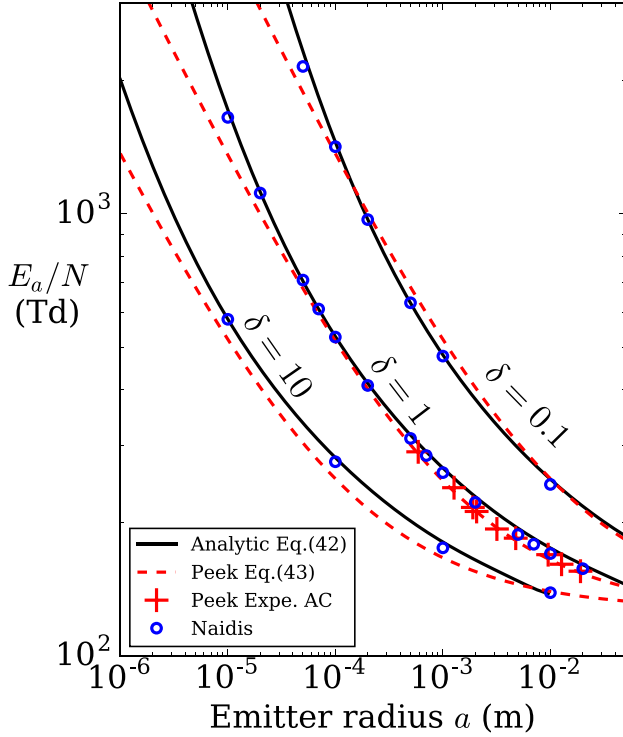


FIG. 5. Reduced onset field versus emitter radius in air at different densities $\delta = N/N_0$, with $N_0 = 2.5 \times 10^{25}$. Comparison between Peek⁹ and Naidis¹¹ and Eq. (42) with $E_{ief} = CN$ and $\beta_{ef} = BN$, B and C from Table I, and $K = \ln(1 + \gamma^{-1})$ given in Ref. 11.

Outside this range, sensible variations are noticeable. For big wires, typically $a > 1$ cm, the asymptotic solution loses accuracy because it is a $O(\varepsilon)$ approximation. The value of ε at the corona inception point can be used to assert the precision of the asymptotic approach as shown in Fig. 6. Using (42) and $\varphi_{on} = aE_a \ln(L/a)$ give the value $\varepsilon_{on} = \varphi_{on}/(LE_i)$

$$\varepsilon_{on} = \hat{a}/\ln(1/\hat{a}) \left[\mathcal{W}_0 \frac{\hat{a}L\beta_{ef}}{\ln(1 + \gamma^{-1})} \right]^{-1}. \quad (44)$$

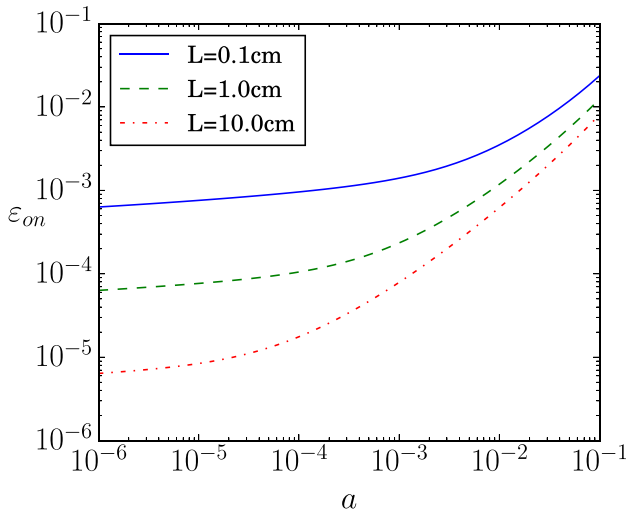


FIG. 6. Asymptotic parameter ε_{on} versus emitter radius $\hat{a} = a/L$ at the corona inception point.

But, the main reason probably relies in the approximation made concerning the functional form of α_{ef} at a low electric field (see Sec. III C 1).

In the submillimeter range, the general criterion (29) is more relevant than Peek's law for two reasons. First, Peek's empirical law was calibrated with experiments for relatively large emitters (see Fig. 5). Second, Peek's law can be theoretically retrieved by quadratically approximating the ionization coefficient $\alpha_{ef}(E)$.¹³ This approximation fails for small wires because of the particular shape of α_{ef} at a high electric field. This is confirmed by the Naidis onset criterion¹¹ for $a < 10 \mu\text{m}$. Since expression (35) relies on a direct integration, it takes full consideration of the non-linear behavior of α_{ef} , especially at high E/N . Hence, (42) matches very well with the Naidis onset criterion, despite the fact that a slightly different value of α_{ef} was used. Besides, (42) can easily be applied to other gases and various densities N , since $\beta = BN$ and $E_i = CN$ with B and C gas constants. This statement must be tempered by the fact that the value of γ is not well established. However, in air, Naidis¹¹ provides the integral $K = \ln(1 + \gamma^{-1})$ for various thermodynamic conditions.

One limitation comes from the evaluation of the secondary electron emission coefficient γ which is poorly documented. This coefficient can encapsulate several physical processes such as wall ion-bombardment (for high energy positive ions in negative coronas), photoelectric emission at the surface of the collector, and photoionization or detachment from negative ions.^{2,27} For large electrode gaps L , we assume that photo-ionization is dominant. For small gaps, of the same order as the absorption length $1/\lambda$, the secondary emission process could change because the collector surface would be exposed to radiation and strong ion flux. In such a case, γ could depend on the collector material work function. A typical value of $\lambda = N \times 8.02 \times 10^{-18} \text{ cm}^{-1}$ (Ref. 27) gives a typical absorption length around $1/\lambda \approx 500 \mu\text{m}$ at atmospheric pressure in air ($N = 2.5 \times 10^{19} \text{ cm}^{-3}$). In more recent publications,^{11,22} multiple ionizing radiation is considered, with a typical maximum absorption length of up to 1 mm.

2. I-V curve

Using (39), (13), and (A2) and rearranging the solution give the dimensional current-voltage I - V law

$$I = \frac{k \varphi_{on}^2}{L^2 \ln\left(\frac{L}{a}\right)^2} \mathcal{F} \left(-2e^{-2} \left(\frac{a}{L} \right)^{\frac{\varphi_a}{\varphi_{on}} - 1} \right), \quad (45)$$

with $k = 2\pi\mu_p\epsilon_g$ and $\varphi_{on} = aE_a \ln(L/a)$ \mathcal{F} given by (40). This law gives the evolution of current per unit length I (A/m) with the applied voltage φ_a . The condition of zero current is still written as $\varphi_a = \varphi_{on}$. It is interesting to compare this law with the Townsend law¹⁹ $I = C_g \varphi_a (\varphi_a - \varphi_{on})$, where C_g is an empirical constant depending on the gas and the electrode geometry. For coaxial cylinders in the low current approximation, Townsend's law is written as⁴

$$C_g = \frac{8\pi\mu_p\epsilon_0}{L^2 \ln(L/a)}. \quad (46)$$

In some works,²⁸ the prefactor is halved, but obviously, using 4π instead of 8π does not match with experiments. Figure 8 shows that the asymptotic expression (45) matches Townsend's law at low voltages. However, at high voltages, the Townsend law underestimates current. This is not surprising since it is a "low current" approximation. To our knowledge, the "low current" condition is not well defined. Here, we propose a simple justification of this approximation and assess its validity range. Consider the first term of the Taylor expansion (41). This linearized non-dimensional law is written as $J = -4(A - \frac{1}{\ln(1/\hat{a})})$. By substituting $J = \frac{IL^2}{2\pi\epsilon_0\mu_p\varphi_a^2}$ and $A = \frac{aE_a}{\varphi_a}$, it is remarkable that the resulting approximated current-voltage law exactly matches the Townsend expression

$$I = \frac{8\pi\mu_p\epsilon_0}{L^2 \ln(L/a)} \varphi_a(\varphi_a - \varphi_{on}), \quad (47)$$

with $\varphi_{on} = aE_a \ln(L/a)$. In other words, Townsend's law is the first order approximation of the asymptotic solution and its validity range can be assessed with the second order term in (41), which scales as $\ln(a/L)^2$. The smaller the reduced emitter radius, the weaker the Townsend approximation.

C. Comparison with experimental results

1. Estimation of effective ionization

In order to derive the analytical expression (35), it is tempting to neglect the attachment η in the matching condition (29). In the following, it is shown that it is an acceptable approximation for the calculation of E_a at very low density and for small corona wires only. The matching condition (29) is rewritten as

$$K = \int_a^\infty \alpha dr [1 - f(a, E_a)], \quad (48)$$

with $f(a, E_a) = \int_a^\infty \eta dr / \int_a^\infty \alpha dr$. $f(a, E_a)$ is *a priori* small quantity because $\eta \ll \alpha$ in a high reduced electric field. And, the smaller the corona wire, the higher, the onset reduced electric field $E_n = E/N$. By changing the integration variable to $E_n(r) = aE_{na}/r$, and because it is in the inner region, f is then written as a function of the surface electric field only

$$f(E_{na}) = \frac{\int_0^{E_{na}} \eta(E_n)/E_n^2 dE_n}{\int_0^{E_{na}} \alpha(E_n)/E_n^2 dE_n}. \quad (49)$$

From the measured ionization and attachment coefficients, it is now obvious that f will be small for large E_{na} . Now, writing this in non-dimensional variables ($\hat{N} = L^3 N$), the asymptotic gives the scaling $\hat{E}_{na} = A/(\hat{N}\hat{a}) \sim 1/(\hat{N}\hat{a})$. So, f can be rewritten as $f \approx \delta_{Na} g(E_{na})$ with $g \sim O(1)$ an order one quantity and

$$\delta_{Na} = \frac{\int_0^{1/\hat{N}\hat{a}} \eta(\hat{E}_n)/\hat{E}_n^2 d\hat{E}_n}{\int_0^{1/\hat{N}\hat{a}} \hat{\alpha}(\hat{E}_n)/\hat{E}_n^2 d\hat{E}_n}. \quad (50)$$

This parameter is a measure of the dominance of α over η in the inner region. It should be small when $Na \rightarrow 0$, because the ionization coefficient dominates the attachment in a high electric field. In air, CO_2 or pure N_2 is in the limit $Na = 0$, it is equal to $\delta_0 \approx 10^{-2}$, while for pure O_2 , the attachment is larger and $\delta_0 \approx 0.1$. Performing the asymptotic analysis by injecting $\hat{E}_a = \hat{E}_{a0} + \delta_{Na}\hat{E}_{a1} + \dots$ into (48) gives

$$K = \int_a^\infty \hat{\alpha}(\hat{E}_{a0}) d\hat{r} + \delta_{Na} \left[\int_a^\infty \frac{d\hat{\alpha}}{d\hat{E}} \Big|_{\hat{E}_{a0}} \hat{E}_{a1} d\hat{r} - g(\hat{E}_{a0}) \right] + O(\delta_{Na}^2).$$

The leading order term is exactly condition (29) without attachment. This simplified condition gives the parameter \hat{E}_{a0} , which is an approximation of the exact \hat{E}_a with accuracy $O(\delta_{Na})$. In a nutshell, neglecting the attachment is relevant if $L^2 Na \rightarrow 0$, e.g., very small wires at low density discharge. In practice, this is not often the case, in typical corona experiments, $\delta_{Na} \simeq 0.5$ is not small enough.

As a consequence, we need to find a functional form for the effective ionization. It is assumed that it takes the form

$$\alpha_{ef}/N = B_{ef} e^{-\frac{C_{ef}}{E/N}}, \quad (51)$$

with N being the gas number density. This formulation is quite convenient because knowing B_{ef} and C_{ef} allows to easily compute the value of α_{ef} for any gas density with the simple conversion $\beta_{ef} = B_{ef} \times N$ and $E_{ief} = C_{ef} \times N$. The ratio E/N is given in Townsend (Td) units with $1 \text{ Td} = 10^{-21} \text{ V m}^2$. Even though other analytical forms exist in low or high electric fields,^{11,12,29} this form has the advantage to cover a wide range of E/N and is justified by the fact that α dominates η . The coefficients are obtained by linearly fitting the data obtained with the Bolsig+ solver.³⁰ The calculations were run from the online cross-section databases.³⁶ Figure 7 shows that in the range 150 and 700 Td, the effective ionization coefficient is well described by an equation similar to (51). This approximation and the chosen fitting range are satisfying for the experiment presented in Table II. In practice, even when the electric field is higher than 700 Td, it remains a good approximation. From (42), we can see that the correct evaluation of the constant E_{ief} is most critical.

2. Experimental current-voltage curves

The cylindrical symmetry simplifies the mathematical resolution, but in the experimental point of view, it is quite sensitive to emitter centering and makes the optical access difficult. Hence, most corona experiments focus on point-to-plane, wire-to-plate or parallel wire-to-cylinder geometries. Some studies did, however, use the coaxial geometry to characterize the corona discharge since theoretical implicit laws are available.^{1,2,5,19,21} These theoretical laws are used to

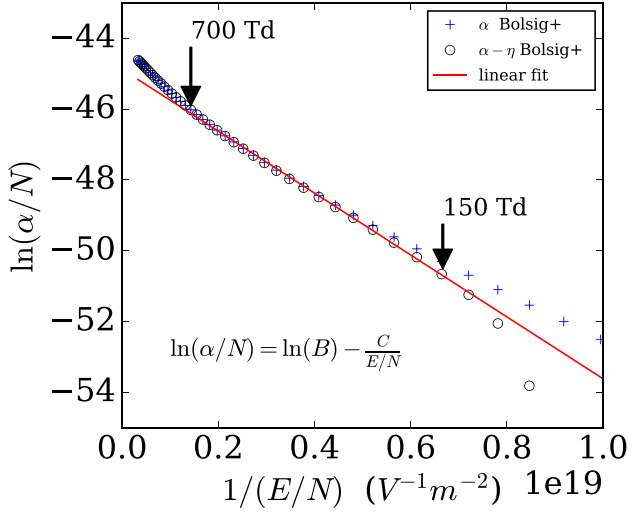


FIG. 7. Linear fit of $\ln(\alpha_{ef})$ in synthetic air $80N_2 + 20O_2$.

recover effective parameters, such as mobility or onset electric field. Given the complex corona ion chemistry, making mobility predictions is uncertain. Indeed, μ_p depends on the gas composition, humidity, and more generally on vapor contaminant.^{31–33} That is why, it is often retrieved by fitting experimental current-voltage curves³⁴ with Townsend’s expression (29). While being rather simple, this method tends to overestimate the mobility value.³ A more advanced method⁵ relies on implicit laws with the concept of the ionization radius, but then the fitted mobility depends on the chosen radius definition.

In the following, expression (45) is compared to experimental and numerical results. Since the effective ionization coefficient is relatively well known for a given gas, see Sec. III C 1, and the only adjustable parameters are μ and $K = \ln(1 + \gamma^{-1})$. The mobility determines the “slope,” while the secondary efficiency controls the inception voltage φ_{on} . The particular case of corona discharge in air has already been extensively studied. In a recent investigation, Zheng *et al.*¹² numerically solved the three species corona model, which they call it the “general fluid model,” for cylindrical axisymmetric electrodes. For the positive corona, they find that the mobility $\mu_p = 1.9 \text{ cm}^2 \text{ V}^{-1} \text{ s}^{-1}$ and the surface electric field $E_a = 65.478 \text{ kV/cm}$ are in excellent agreement with experiment.

Now, in order to assess the validity of the analytical solution, the previous parameters were injected into Eq. (45).

The electric field prescribed by Zheng corresponds to an inception voltage $\varphi_{on} = 22.878 \text{ kV}$. The comparison between Zheng’s experimental data (and so the numerical solution of the model) is shown in Fig. 8 and shows excellent agreement. Furthermore, this value of the mobility is close to the precise ion mobility measurement made by Stearn³ in a positive DC corona $\mu_p = 1.8 \text{ cm}^2 \text{ V}^{-1} \text{ s}^{-1}$. The small difference is very probably due to different temperature and pressure conditions between Zheng and Stearns setups. Fitting the values of Zheng *et al.*¹² gives $\mu = 1.86 \text{ cm}^2 \text{ V}^{-1} \text{ s}^{-1}$.

For the experiments in pure oxygen gas, shown in Fig. 9, performed by Yanallah *et al.*,⁶ μ_p and γ are obtained by fitting to experimental data. The mobility is much larger than in air, probably because there is less ion clustering in a high purity gas resulting in small ions such as O_2^+ . The corona inception field is higher in pure oxygen, resulting in a lower secondary ionization efficiency. The comparison of those results would be fully relevant to pressure and temperature corrections, but the experimental conditions are not always given in the published works.

Horvath *et al.*³⁴ investigated the influence of a small amount of CH_4 in N_2 gas, shown as Fig. 10. Once again, the theoretical law can be adjusted to the experimental data. The presence of a small amount of CH_4 results in a smaller mobility value and a smaller secondary coefficient. The lower mobility is consistent with the larger ions generated by ionized CH_4 molecules. The theoretical curves very favorably compare with experiments, even if a small discrepancy is observed for pure N_2 gas at high voltages.

The experimental parameters and fitted values are gathered in Table II. They favorably compare with experimental mobility values.³⁷ In those experiments, the parameter $\hat{a} = a/L$ is rather small, between 0.005 and 0.008, which illustrates the low accuracy of Townsend’s law far from the inception point.

IV. DISCUSSION

A. Practical example

The previous simplified model of the corona discharge allows to quickly investigate the influence of each parameter. In planar gas discharge, a figure of merit is Paschen’s law. This law governs the breakdown voltage as a function of the parameter $N \times d$ (or classically $P \times d$), for parallel plates separated by a distance d at gas number density N (or classically

TABLE II. Experimental conditions and fitted values of γ and μ_p . When experimental pressure and temperature are not given, standard conditions are used: $P_0 = 1013 \text{ hPa}$ and $T_0 = 293 \text{ K}$.

	Air ¹²	O_2 (Ref. 6)	N_2 (Ref. 34)	$98N_2 + 2CH_4$ (Ref. 34)
P_0 (Pa)	1010×10^2
T_0 (K)	298
E_i (V m^{-1})	2.09×10^7	1.99×10^7	2.12×10^7	2.16×10^7
β (m^{-1})	7.20×10^5	1.15×10^6	6.35×10^5	7.26×10^5
L (m)	1.03×10^{-1}	1.10×10^{-2}	8.00×10^{-3}	8.00×10^{-3}
a (m)	7.00×10^{-4}	6.25×10^{-5}	6.25×10^{-5}	6.25×10^{-5}
γ (-)	2×10^{-3}	1×10^{-6}	5×10^{-4}	4×10^{-5}
μ_p ($\text{m}^2 \text{ V}^{-1} \text{ s}^{-1}$)	1.86×10^{-4}	2.47×10^{-4}	2.25×10^{-4}	1.56×10^{-4}

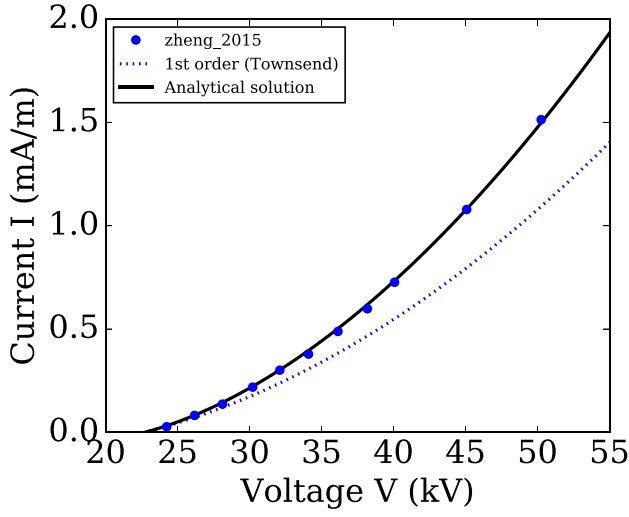


FIG. 8. Current voltage characteristic in ambient air from Zheng.¹²

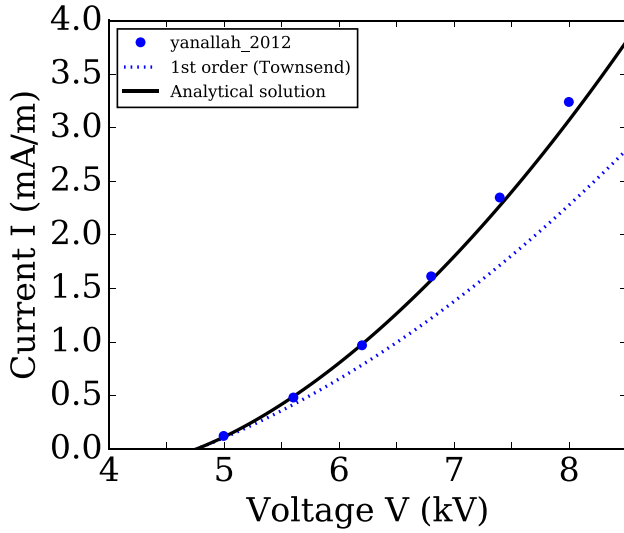


FIG. 9. Current voltage characteristic in pure oxygen from Yanallah.⁶

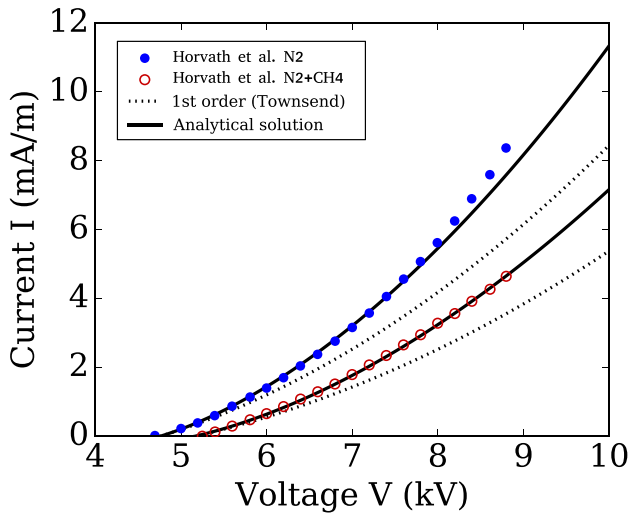


FIG. 10. Current voltage characteristic in pure N_2 gas and the N_2 - CH_4 (98:2) mixture from Horvath *et al.*³⁴

pressure P). Paschen's law directly derived from Townsend's criterion applies to planar electrodes²⁸

$$V_{b,plate} = \frac{C \times Nd}{\ln(B \times Nd / \ln(1 + \gamma^{-1}))}, \quad (52)$$

with $V_{b,plate}$ being the voltage at which the Townsend breakdown criterion is fulfilled. The onset of corona discharge can be seen as a local gas breakdown, or partial breakdown, nearby the emitter. Injecting the condition $V_{b,cyl} = E_a a \ln(L/a)$ into expression (42) gives the corona onset law for cylindrical electrodes

$$\frac{V_{b,cyl}}{\ln(L/a)} = \frac{C \times Na}{\mathcal{W}_0(B \times Na / \ln(1 + \gamma^{-1}))}. \quad (53)$$

The analogy with the classical Paschen's law is striking. The parameter Nd is changed to Na , the logarithm by the Lambert W function and a geometric correction factor $\ln(L/a)$ appears. But, the corona onset curve in cylindrical geometry shown in Fig. 11 fundamentally differs from the planar Paschen curve. Indeed, for a corona discharge in air, the secondary electron emission process depends on the quenching of emitting states of nitrogen molecules, which breaks the dependency on Na .¹¹ In other words, $\frac{V_{b,cyl}}{\ln(L/a)}$ depends on a and N separately.

No minimum is apparently visible for the corrected breakdown voltage $V_{b,cyl}/\ln(L/a)$. But, there is a minimum for $V_{b,cyl}$ as a decreases. The radius for the minimum breakdown voltage a_{min} can be obtained by differentiating (53) with respect to a and looking for zero. In practice, at atmospheric pressure, a_{min} is around a few microns. When Na is very small, the expression can be approximated by linearizing the Lambert function $\mathcal{W}_0(x) \sim x$, when $x \rightarrow 0$

$$\frac{V_{b,cyl}}{\ln(L/a)} \sim \frac{C}{B} \ln(1 + \gamma^{-1}). \quad (54)$$

The condition to reach this regime is written as $Na \ll \ln(1 + \gamma^{-1})/B \approx 10^{20}$, which corresponds at atmospheric

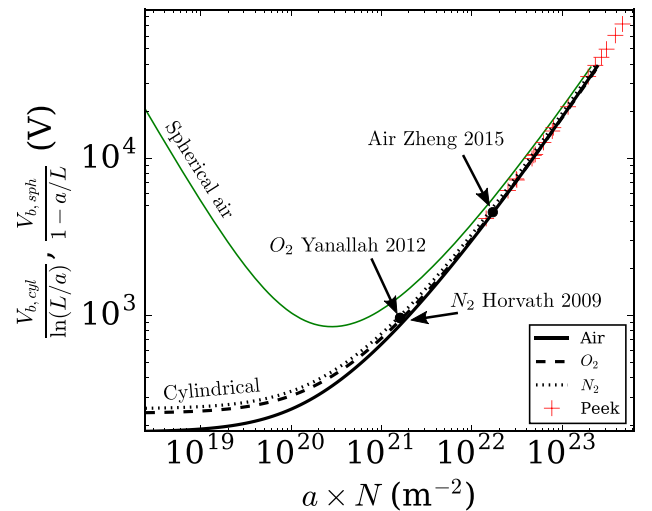


FIG. 11. Corona onset curve for cylindrical Eq. (53) and spherical (29) electrodes in air at $N/N_0 = 1$.

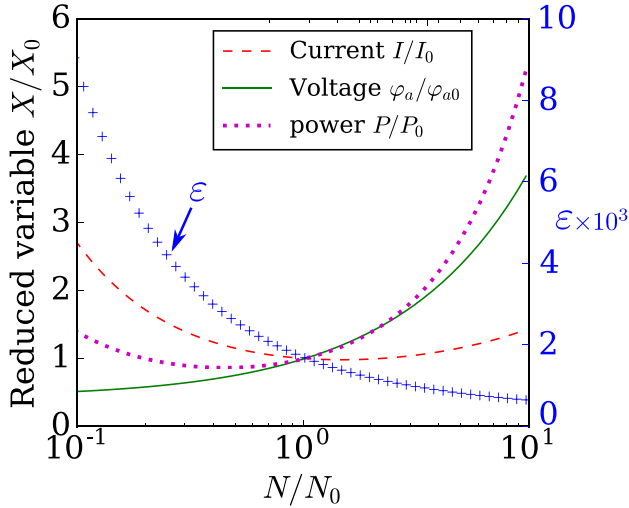


FIG. 12. Current, voltage and power normalized with their value at $N_0 = 2.5 \times 10^{25} \text{ m}^{-3}$ (lines, left axis) and the asymptotic parameter $\varepsilon = \varphi_a/LE_i$ (crosses, right axis).

pressure in air to an emitter smaller than $5 \mu\text{m}$. Figure 11 illustrates this asymptote and the position of a typical experimental corona realized at atmospheric pressure. In practice, this regime could concern miniaturized corona devices, such as ionic wind cooling devices.

It is tempting to extrapolate the asymptotic approach to the spherical case. But, despite our efforts, no explicit analytical solution was found for the matching conditions. In Fig. 11, we solve numerically the onset criterion (29) with an inner voltage gradient of type $\partial_R \Phi = A/R^2$.

Another parametric use of the asymptotic model is illustrated in Fig. 12. It shows the evolution of current, voltage and power consumption with gas density for a small corona wire. The input parameters are $L = 10 \text{ cm}$ and $a = 10 \mu\text{m}$, and the mobility is assumed to be inversely proportional to air density $\mu_p = \mu_{p0}N_0/N$. The applied voltage is assumed to depend on the inception voltage, so that the voltage ratio is constant $\varphi_a = 1.5\varphi_{on}$. But power consumption and net corona current both exhibit minima at different locations.

The two previous applicative examples of this analytical model illustrate its interest when exploring the parameter space with the two matching equations (42) and (45). Some limitations of the model can be anticipated:

1. The validity range of shape (51) for α_{ef} . In the previous example at low gas density $N/N_0 = 0.1$, the reduced electric field at the wire surface was $E/CN \approx 6$, far above typical values for CD under standard conditions.
2. The asymptotic parameter $\varepsilon = \varphi_a/LE_i$ should remain small.
3. In practice, the secondary ionization process $K = \ln(1 + \gamma^{-1})$ is mainly documented in air, but not in other gases.

V. CONCLUSION

We revisit the theoretical analysis of the positive DC corona using asymptotic matching without much noticeable changes to Ref. 1, but to get some clarification in the

derivation, including attachment, and much more importantly, explicit analytical solutions for the matching conditions. These dimensionless formulations are then transformed into the dimensional onset electric field (42), expressed as explicit functions of the gas ionization properties and electrode size and dimensional current (45), expressed as an explicit function of mobility, onset voltage and electrode size. Both results are independent of each other and can be used separately. This is, to our knowledge, the first time that an explicit analytical expression of the current voltage law is derived.

First, concerning the onset criterion:

- Despite the simplified form of α_{ef} , the onset field matches well with the more sophisticated onset criterion in air.
- The analytical onset voltage for cylindrical electrodes is recovered. A surprising analogy is found with Paschen's law for breakdown between plane electrodes.

Then, concerning the “shape” of the current voltage curve:

- The analytical model successfully predicts corona current in air. It perfectly matches the numerical solution performed by Zheng for the very same equations and experiments.
- The low current approximation of the non-dimensional analytical solution is linear with a universal slope of -4 and is written as $J = -4(A + 1/\ln(\hat{a}))$. In dimensional variables, it exactly matches Townsend's expression.
- The validity range of Townsend's law is assessed depending on the parameter $\ln(a/L)^2$. Townsend's approximation loses accuracy for small emitting corona electrodes.

This analytical approach can easily be used to determine the onset voltage and ion mobility. It also provides a good reference for testing new numerical algorithms dedicated to corona current predictions with much better accuracy than Townsend's law. The analytical solution is helpful for exploring new corona applications, especially with small corona wires. Finally, we would like to mention that, regarding the (rather complete) present state-of-the-art of corona discharge modeling, the advantage of the presented asymptotic approach over previously cited (more phenomenological) models might not seem obvious. From the practical view point, the presented theoretical development is mainly supporting previous approaches rather than challenging them, although it can be applied to any thermodynamic conditions and gases. However, we would like to stress that the generality of the presented theoretical framework encompasses the hereby studied example. It has potential to model the complex coupling between corona discharges and drift regions in much more complex configurations. This is the perspective of future research efforts.

ACKNOWLEDGMENTS

The authors thank the French Space Agency CNES and Region Occitanie for financial support and L. Pitchford and J. P. Boeuf for introducing the LXcat project. This research was funded by CNES research Contract No. 5100015475.

APPENDIX A: DETAILS OF THE ASYMPTOTIC MATCHING FOR THE ELECTRICAL POTENTIAL

The matching on potential is performed with an intermediate variable η . It is a three-step procedure:

- (i) Expressing the inner and outer solutions in an intermediate zone $\eta = \hat{r}/\varepsilon^\kappa = R\varepsilon^{1-\kappa}$ with $0 < \kappa < 1$.
 - (ii) Expanding $\Phi(\eta)$ and $\hat{\varphi}(\eta)$ in the limit $\varepsilon \rightarrow 0$, which corresponds to $R \rightarrow \infty$ and $\hat{r} \rightarrow 0$.
 - (iii) Comparing the inner and outer expansions term by term. The equalization of each term gives a matching condition.
- (i) The inner solution is written as

$$\Phi(R) = 1 - \text{A} \ln\left(\frac{R}{\hat{a}/\varepsilon}\right). \quad (\text{A1})$$

The inner boundary condition $\Phi_a = 1$ has already been applied and A is a constant to determine by the electron matching condition, see (35). A can be interpreted as the non-dimensional surface electric field

$$A = -\hat{a}/\varepsilon(\partial_R\Phi)|_a = -\hat{a}(\partial_{\hat{r}}\hat{\varphi})|_a = \frac{aE_a}{\varphi_a}. \quad (\text{A2})$$

The outer solution is obtained in two steps. First, integration of (23) with $\hat{\pi}_p = \hat{n}_p\hat{r}\partial_{\hat{r}}\hat{\varphi} = 1$ gives the electric field flux

$$(\hat{r}\partial_{\hat{r}}\hat{\varphi})^2 = J\hat{r}^2 + K_1. \quad (\text{A3})$$

Integrating again gives the electric potential in the outer region

$$\hat{\varphi}(\hat{r}) = -\sqrt{J\hat{r}^2 + K_1} + \sqrt{K_1} \ln\left(\frac{\sqrt{J\hat{r}^2 + K_1} + \sqrt{K_1}}{\sqrt{J\hat{r}^2}}\right) + K_2.$$

The constant K_2 can be determined by the outer boundary condition $\hat{\varphi}(1) = 0$

$$K_2 = \sqrt{J + K_1} - \sqrt{K_1} \ln\left(\frac{\sqrt{J + K_1} + \sqrt{K_1}}{\sqrt{J}}\right). \quad (\text{A4})$$

The outer solution is written as

$$\hat{\varphi}(\hat{r}) = \sqrt{J + K_1} - \sqrt{J\hat{r}^2 + K_1} + \sqrt{K_1} \ln\left(\frac{\sqrt{J\hat{r}^2 + K_1} + \sqrt{K_1}}{\hat{r}(\sqrt{J + K_1} + \sqrt{K_1})}\right). \quad (\text{A5})$$

Now, rewriting the previous expressions with the intermediate variable $\eta = \hat{r}/\varepsilon^\kappa = R\varepsilon^{1-\kappa}$ with $0 < \kappa < 1$ leads to

$$\begin{aligned} \varphi(\eta) &= 1 - \text{A} \ln\left(\frac{\eta\varepsilon^\kappa}{a}\right) + \varepsilon\varphi_1 + \dots \\ \Phi(\eta) &= \sqrt{J + K_1} - \sqrt{J\varepsilon^{2\kappa}\eta^2 + K_1} \\ &\quad + \sqrt{K_1} \ln\left(\frac{\sqrt{J\varepsilon^{2\kappa}\eta^2 + K_1} + \sqrt{K_1}}{\varepsilon^\kappa\eta(\sqrt{J + K_1} + \sqrt{K_1})}\right) + \varepsilon\Phi_1 + \dots \end{aligned}$$

- (ii) The previous expression is expanded in the limit $\varepsilon \rightarrow 0$ at fixed η . To perform the matching, it is more convenient to reorganize the terms from the dominant one in $\ln(\varepsilon)$ to the weaker one ε^0

$$\begin{aligned} \Phi \underset{\varepsilon \rightarrow 0}{\sim} & -\sqrt{K_1}\kappa \ln(\varepsilon) + \sqrt{J + K_1} - \sqrt{K_1} \\ & + \sqrt{K_1} \ln\left(\frac{2\sqrt{K_1}}{\eta(\sqrt{J + K_1} + \sqrt{K_1})}\right) + O(\varepsilon \ln \varepsilon) \underset{\varepsilon \rightarrow 0}{\varphi} \sim -A\kappa \ln(\varepsilon) \\ & + 1 - \text{A} \ln\left(\frac{\eta}{a}\right) + O(\varepsilon \ln \varepsilon). \end{aligned}$$

The $O(\varepsilon \ln \varepsilon)$ term comes from the first order terms $\hat{\varphi}_1$ and $\hat{\Phi}_1$ which are not further detailed here because they are not needed for the leading order solution. (iii) The two series have to match term by term. Matching dominant terms in $O(\ln \varepsilon)$ gives

$$\sqrt{K_1} = A. \quad (\text{A6})$$

Then, matching the terms in ε^0 , while injecting (A6) and simplifying gives

$$1 - \text{A} \ln\left(\frac{1}{\hat{a}}\right) = \sqrt{J + A^2} - A + A \ln\left(\frac{2A}{\sqrt{J + A^2} + A}\right).$$

APPENDIX B: COMPARISON WITH THE CHARGE INJECTION MODEL OF ZHENG *ET AL.*

Usually, the relation between current and voltage is retrieved with a charge injection model such as the ‘‘ion flow model’’ described by Zheng *et al.*¹² In the following, the precise comparison with the hereby developed asymptotic model is discussed. In the charge injection model, the electric field can be analytically expressed as

$$E(r) = \sqrt{\frac{I}{2\pi\varepsilon_0\mu} \left(1 - \frac{a^2}{r^2}\right) + \left(\frac{aE_a}{r}\right)^2} \quad (\text{B1})$$

and the current I is then given by the condition on electric potential

$$\varphi(a) - \varphi(L) = \int_a^L E(r) dr. \quad (\text{B2})$$

The non-dimensional expression of condition (B2)

$$1 = \int_{\hat{a}}^1 \sqrt{J \left(1 - \frac{\hat{a}^2}{\hat{r}^2}\right) + \frac{A^2}{\hat{r}^2}} d\hat{r} \quad (\text{B3})$$

or equivalently

$$V = \frac{1}{\ln(1/\hat{a})} \int_{\hat{a}}^1 \sqrt{C \left(1 - \frac{\hat{a}^2}{\hat{r}^2}\right) + \frac{1}{\hat{r}^2}} d\hat{r} \quad (\text{B4})$$

is similar to the matching condition of Durbin and Turyn, but with an additional term $J\hat{a}^2/\hat{r}^2$. This additional term, which is small since it scales as \hat{a}^2 , is the consequence of the

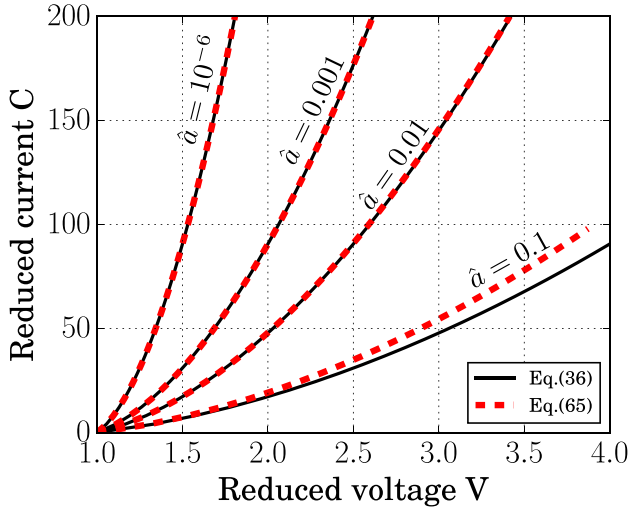


FIG. 13. Current with the charge injection and the asymptotic model, for different emitter sizes.

charge injection directly at the surface of the emitter, while for the asymptotic approach, the “injection” occurs at the edge (intermediate zone) of the ionization layer. Both approaches give similar results for small values of \hat{a} , typically for most corona applications. Indeed, performing the integration of Eq. (B4) leads to

$$V = \sqrt{1 - \hat{a}^2 C} + \frac{1}{\ln(1/\hat{a})} \left[-1 + \sqrt{C + 1 - \hat{a}^2 C} + \sqrt{1 - \hat{a}^2 C} \ln \left(\frac{\sqrt{1 - \hat{a}^2 C} + 1}{\sqrt{1 - \hat{a}^2 C} + \sqrt{C + 1 - \hat{a}^2 C}} \right) \right], \quad (\text{B5})$$

which exactly match the asymptotic result given by Eq. (36), for $\hat{a} \rightarrow 0$. The reduced current voltage curves are compared in Fig. 13. No difference is visible for reasonably small corona wires $\hat{a} \leq 0.01$.

- ¹P. Durbin and L. Turyn, “Analysis of the positive DC corona between coaxial cylinders,” *J. Phys. D: Appl. Phys.* **20**, 1490–1495 (1987).
- ²R. G. Stearns, “The positive corona in air: A simplified analytic approach,” *J. Appl. Phys.* **66**(7), 2899–2913 (1989).
- ³R. G. Stearns, “Ion mobility measurements in a positive corona discharge,” *J. Appl. Phys.* **67**(6), 2789–2799 (1990).
- ⁴R. S. Sigmond, “Simple approximate treatment of unipolar space-charge-dominated coronas: The Warburg law and the saturation current,” *J. Appl. Phys.* **53**(2), 891–898 (1982).
- ⁵J. E. Jones, J. Dupuy, G. O. S. Schreiber, and R. T. Waters, “Boundary conditions for the positive direct-current corona in a coaxial system,” *J. Phys. D: Appl. Phys.* **21**(2), 322–333 (1988).
- ⁶K. Yanallah, F. Pontiga, Y. Meslem, and A. Castellanos, “An analytical approach to wire-to-cylinder corona discharge,” *J. Electrostat.* **70**(4), 374–383 (2012).
- ⁷M. J. Johnson and D. B. Go, “Recent advances in electrohydrodynamic pumps operated by ionic winds: A review,” *Plasma Sources Sci. Technol.* **26**(10), 103002 (2017).
- ⁸N. Monrolin, F. Plouraboué, and O. Praud, “Electrohydrodynamic thrust for in-atmosphere propulsion,” *AIAA J.* **55**(12), 4296–4305 (2017).

- ⁹F. W. Peek, *Dielectric Phenomena in High Voltage Engineering* (McGraw-Hill Book Company Inc., 1915), Chap. 3, pp. 38–78.
- ¹⁰S. Z. Li and H. S. Uhm, “Investigation of electrical breakdown characteristics in the electrodes of cylindrical geometry,” *Phys. Plasmas* **11**(6), 3088 (2004).
- ¹¹G. V. Naidis, “Conditions for inception of positive corona discharges in air,” *J. Phys. D: Appl. Phys.* **38**(13), 2211–2214 (2005).
- ¹²Y. Zheng, B. Zhang, and J. He, “Current-voltage characteristics of dc corona discharges in air between coaxial cylinders,” *Phys. Plasmas* **22**(2), 023501 (2015).
- ¹³J. J. Lowke and F. D’Alessandro, “Onset corona fields and electrical breakdown criteria,” *J. Phys. D: Appl. Phys.* **36**(21), 2673–2682 (2003).
- ¹⁴J. J. Lowke and R. Morrow, “Theory of electric corona including the role of plasma chemistry,” *Pure Appl. Chem.* **66**(6), 1287–1294 (1994).
- ¹⁵P. Seimandi, G. Dufour, and F. Rogier, “An asymptotic model for steady wire-to-wire corona discharges,” *Math. Comput. Modell.* **50**(3–4), 574–583 (2009).
- ¹⁶P. Seimandi, G. Dufour, and F. Rogier, “A two scale model of air corona discharges,” *Procedia Comput. Sci.* **1**(1), 627–635 (2010).
- ¹⁷H. Shibata, Y. Watanabe, and K. Suzuki, “Performance prediction of electrohydrodynamic thrusters by the perturbation method,” *Phys. Plasmas* **23**(5), 053512 (2016).
- ¹⁸H. Shibata and R. Takaki, “A novel method to predict current voltage characteristics of positive corona discharges based on a perturbation technique. I. Local analysis,” *AIP Adv.* **7**, 115026 (2017).
- ¹⁹J. S. Townsend and P. J. Edmunds, “The discharge of electricity from cylinders and points,” *Philos. Mag. Ser. 6* **27**(161), 789–801 (1914).
- ²⁰J. S. Townsend, *Electricity in Gases* (Clarendon Press, 1915).
- ²¹J. Feng, “An analysis of corona currents between two concentric cylindrical electrodes,” *J. Electrostat.* **46**(1), 37–48 (1999).
- ²²Y. Zheng, B. Zhang, and J. He, “Self-sustained criterion with photoionization for positive dc corona plasmas between coaxial cylinders,” *Phys. Plasmas* **22**(6), 063514 (2015).
- ²³G. W. Penney and G. T. Hummert, “Photoionization measurements in air, oxygen, and nitrogen,” *J. Appl. Phys.* **41**(2), 572–577 (1970).
- ²⁴E. J. Hinch, *Perturbation Methods*, Cambridge Texts in Applied Mathematics (Cambridge University Press, 1991).
- ²⁵R. T. Waters and W. B. Stark, “Characteristics of the stabilized glow discharge in air,” *J. Phys. D: Appl. Phys.* **8**, 416–426 (1975).
- ²⁶R. M. Corless, G. H. Gonnet, D. E. G. Hare, D. J. Jeffrey, and D. E. Knuth, “On the Lambert W function,” *Adv. Comput. Math.* **5**(1), 329–359 (1996).
- ²⁷J. M. Meek and J. D. Craggs, *Electrical Breakdown of Gases* (Oxford University Press, 1953), Chap. 1, pp. 1–78.
- ²⁸J. R. Roth, *Industrial Plasma Engineering, Principles* (IOP Publishing Ltd., London, 1995), Vol. 1, Chap. 8, pp. 237–282.
- ²⁹R. Morrow, “The theory of positive glow corona,” *J. Phys. D: Appl. Phys.* **30**, 3099–3114 (1997).
- ³⁰G. J. M. Hagelaar and L. C. Pitchford, “Solving the Boltzmann equation to obtain electron transport coefficients and rate coefficients for fluid models,” *Plasma Sources Sci. T* **14**(4), 722–733 (2005).
- ³¹M. L. Huertas, A. M. Marty, J. Fontan, and G. Duffa, “Measurement of mobility and mass of atmospheric ions,” *J. Aerosol. Sci.* **2**, 145–150 (1971).
- ³²M. L. Huertas and J. Fontan, “Evolution times of tropospheric positive ions,” *Atmos. Environ.* **9**, 1018–1026 (1975).
- ³³N. Fujioka, Y. Tsunoda, A. Sugimura, and K. Arai, “Influence of humidity on variation of ion mobility with life time in atmospheric air,” *IEEE Trans. Power Appar. Syst.* **PAS-102**(4), 911–917 (1983).
- ³⁴G. Horvath, J. D. Skalny, N. J. Mason, M. Klas, M. Zahoran, R. Vladouiu, and M. Manole, “Corona discharge experiments in admixtures of N₂ and CH₄: A laboratory simulation of Titan’s atmosphere,” *Plasma Sources Sci. Technol.* **18**, 034016 (2009).
- ³⁵By definition $\mathcal{W}(ye^y) = y$ for $y \in \mathbb{R}$ and $x = \mathcal{W}(x)e^{\mathcal{W}(x)}$ for $x \geq -1/e$.
- ³⁶See www.lxcat.net for IST-lisbon (N₂, CH₄) and Phelps database (N₂, O₂); accessed 10 October 2017.
- ³⁷See www.lxcat.net for Phelps and Vielhand databases; accessed 10 October 2017.